Biomimetic structures for fluid drag reduction in laminar and turbulent flows

2010 J. Phys.: Condens. Matter 22 035104

(http://iopscience.iop.org/0953-8984/22/3/035104)

IOP Publishing Journal of Physics: Condensed Matter

J. Phys.: Condens. Matter **22** (2010) 035104 (9pp) doi:10.1088/0953-8984/22/3/035104

Biomimetic structures for fluid drag reduction in laminar and turbulent flows

Yong Chae Jung and Bharat Bhushan[1]

Nanoprobe Laboratory for Bio- and Nanotechnology and Biomimetics (NLB^2), The Ohio State University, 201 West 19th Avenue, Columbus, OH 43210-1142, USA

E-mail: Bhushan.2@osu.edu

Received 16 October 2009, in final form 16 November 2009
Published 21 December 2009
Online at stacks.iop.org/JPhysCM/22/035104

Abstract

Biomimetics allows one to mimic nature to develop materials and devices of commercial interest for engineers. Drag reduction in fluid flow is one of the examples found in nature. In this study, nano, micro, and hierarchical structures found in lotus plant surfaces, as well as shark skin replica and a rib patterned surface to simulate shark skin structure were fabricated. Drag reduction efficiency studies on the surfaces were systematically carried out using water flow. An experimental flow channel was used to measure the pressure drop in laminar and turbulent flows, and the trends were explained in terms of the measured and predicted values by using fluid dynamics models. The slip length for various surfaces in laminar flow was also investigated based on the measured pressure drop. For comparison, the pressure drop for various surfaces was also measured using air flow.

1. Introduction

Biologically inspired design or adaptation or derivation from nature is referred to as 'biomimetics'. The understanding of the functions provided by objects and processes found in nature can guide us to imitate and produce nanomaterials, nanodevices and processes (Bhushan 2009). A model surface for superhydrophobicity and drag reduction is provided by the leaves of the lotus plant (*Nelumbo nucifera*), which have an intrinsic hierarchical structure, built by convex cell papillae and randomly oriented hydrophobic wax tubules (Barthlott and Neinhuis 1997, Koch *et al* 2008, 2009a). The lotus plant surface with hierarchical structure has a very high contact angle of 164° and low water contact angle hysteresis (the difference between the advancing and receding contact angles), on the order of 3°, which is responsible for water droplets rolling (with some slip) off the surface and taking contaminants with them, providing a self-cleaning ability known as the lotus effect (Koch *et al* 2009b). Water on such a surface forms a spherical droplet, and both the contact area and the adhesion to the surface are dramatically reduced. Based on the understanding of nature, a number of artificial hydrophobic surfaces have been fabricated with hierarchical structures using electrodeposition, colloidal particles, photolithography, soft lithography, plasma treatment, self-assembly, and imprinting (Shirtcliffe *et al* 2004, Ming *et al* 2005, Sun *et al* 2005, Chong *et al* 2006, del Campo and Greiner 2007, Cortese *et al* 2008, Zhao *et al* 2008, Bhushan *et al* 2009, Koch *et al* 2009b, Kuan *et al* 2009).

Another model surface from nature for a low drag surface is shark skin, which is covered by very small individual tooth-like scales called dermal denticles (little skin teeth), ribbed with longitudinal grooves (aligned parallel to the local flow direction of the water). These grooved scales reduce the formation of vortices present on a smooth surface, resulting in water moving efficiently over their surface (Bechert *et al* 2000, Bhushan 2009). The water surrounding these complex structures can lead to protection from marine fouling and play a role in the defense against adhesion and growth of marine organisms, e.g., bacteria and algae (Genzer and Efimenko 2006, Koch *et al* 2009a).

The study of drag reduction in fluid flow is of interest in micro/nanofluidics based biosensor applications (Bhushan 2007). To reduce pressure drop and volume loss in micro/nanochannels, it is desirable to minimize the drag force in the solid–liquid interface. It is generally assumed that the relative velocity between a solid wall and liquid is zero at the solid–liquid interface, which is the so called no-slip boundary condition (figure 1, left) (Stokes 1851, Batchelor 1970). However, this assumption has been widely debated for hydrophobic surfaces, and fluid film exhibits a phenomenon known as slip, which means that the fluid velocity near the

[1] Author to whom any correspondence should be addressed.

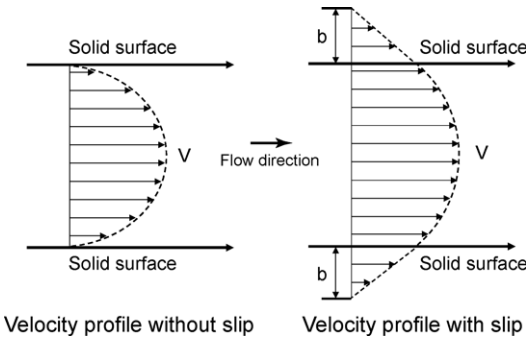

Figure 1. Schematic of velocity profiles of fluid flow without and with boundary slip. The definition of slip length b characterizes the degree of boundary slip at the solid–liquid interface. The arrows represent directions for fluid flow.

solid surface is not equal to the velocity of the solid surface (figure 1, right) (Goldstein 1938, 1969, Lauga *et al* 2005, Neto *et al* 2005, Maali and Bhushan 2008, Wang *et al* 2009). The degree of boundary slip at the solid–liquid interface is characterized by a slip length. Slip length is defined as the length of the vertical intercept along the axis orthogonal to the interface when a tangent line is drawn along the velocity profile at the interface (figure 1, right). Recent experiments with surface force apparatus (SFA) (Baudry *et al* 2001, Zhu and Granick 2002, Cottin-Bizonne *et al* 2005), atomic force microscopy (AFM) (Vinogradova and Yakubov 2003, Wang *et al* 2009), and particle image velocimetry (PIV) (Tretheway and Meinhart 2002) techniques have reported slip lengths on hydrophobic surfaces, and no slip was observed on hydrophilic surfaces (Baudry *et al* 2001, Tretheway and Meinhart 2002, Vinogradova and Yakubov 2003, Cottin-Bizonne *et al* 2005, Honig and Ducker 2007, Maali *et al* 2009). Theoretical studies (Watts *et al* 1990, Lauga and Stone 2003, Cottin-Bizonne *et al* 2004, Sbragaglia and Prosperetti 2007) and experimental studies (Ou *et al* 2004, Choi and Kim 2006, Joseph *et al* 2006) suggest that the presence of nanobubbles at the solid–liquid interface is responsible for boundary slip on hydrophobic surfaces.

In this paper, to investigate drag reduction efficiency on biomimetic structured surfaces, channels with flat, nano, micro, and hierarchical structures, as well as shark skin replica and rib patterned surfaces were created. The pressure drop in the channel was measured using laminar and turbulent water flows, and the trends were explained in terms of the measured and predicted values by using fluid dynamics models. The slip length for various surfaces in laminar flow was also investigated based on the measured pressure drop. For comparison, the pressure drop for various surfaces was also measured using air flow.

2. Experimental details

2.1. Samples

Microstructures were fabricated using a microstructured Si surface with pillars of 14 μm diameter and 30 μm height with 23 μm pitch by soft lithography (Bhushan *et al* 2009, Koch *et al* 2009b). The replication is a two step molding process, in which a negative replica of a template is generated using a polyvinylsiloxane dental wax (President Light Body® Gel, ISO 4823, Polyvinylsiloxan (PLB), Coltene Whaledent, Hamburg, Germany), and a positive replica is made with a liquid epoxy resin (Epoxydharz L®, No. 236349, Conrad Electronics, Hirschau, Germany) with hardener (Harter S, Nr 236365, Conrad Electronics, Hirschau, Germany).

Nanostructures were created by self-assembly of plant wax deposited by thermal evaporation (Bhushan *et al* 2009, Koch *et al* 2009b). Tubule forming wax, which was isolated from a leaf of *Nelumbo nucifera*, in the following referred to as lotus, was used to create tubule structures. Lotus wax with 0.8 μg mm^{-2} was deposited on the specimen surfaces by thermal evaporation. The specimens with lotus wax were exposed to ethanol vapor for three days at 50 °C, and then left in the oven at 50 °C in total for seven days.

Hierarchical structures were fabricated using a two step fabrication process, including the production of microstructured surfaces by soft lithography and subsequent development of nanostructures on top by self-assembly of lotus wax, as described above. The flat epoxy resin and microstructure were covered with flat lotus wax. The flat thin wax layer was made by melting the deposited wax (3 min at 120 °C) and subsequent rapid cooling of the specimen to 5 °C. Then the specimens were stored for seven days at 21 °C in a desiccator. The fast cooling of the wax prevents the formation of nanostructure roughness.

Figure 2 shows the scanning electron microscope (SEM) micrographs of nanostructure on flat replica, microstructures, and hierarchical structure. SEM micrographs show an overview (left column), a detail in higher magnification (middle column), and a large magnification of the created flat wax layers and tubules nanostructures (right column). All surfaces show a homogeneous distribution of the wax mass on the specimen. The recrystallized lotus wax shows tubular hollow structures with random orientation on the surfaces. Their diameter varied between 100 and 150 nm, and their length varied between 1500 and 2000 nm.

A shark (*Squalus acanthias*, L. Squalidae) was used for creating a shark skin replica. The shark is an aquatic creature, and its skin is permanently exposed to contamination from marine organisms, e.g., bacteria and algae. The shark was conserved in FAA (formaldehyde–acetic acid–ethanol) solution. The detailed structure varies from one location to another for the shark. The scales are present over most of the shark's body. To create a replica, the right front of the shark's body was selected. Before replicating the conserved shark skin, the selected area was first cleaned with acetone and then washed with deionized water. This process was repeated twice. The cleaned skin was placed in air for 1 h for drying. For the negative replica, a polyvinylsiloxane dental wax was applied via a dispenser on the upper side of the shark skin and immediately pressed down with a glass plate. After complete hardening of the molding mass (at room temperature 3–5 min), the master surface and the mold (negative) were separated. The first negative replica was made only to remove any remaining contaminations from the shark surface by embedding the dirt

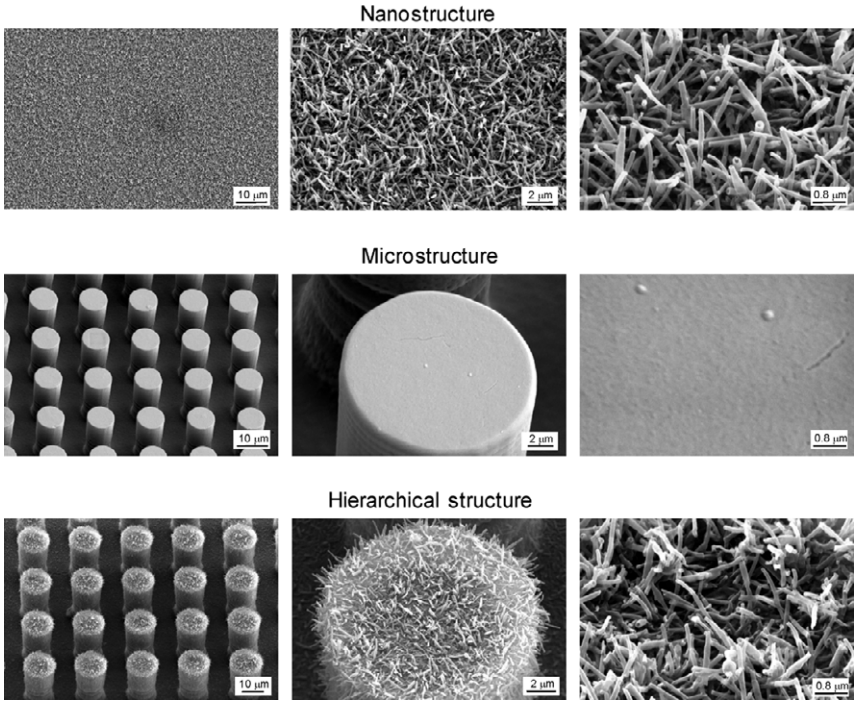

Figure 2. SEM micrographs taken at 45° tilt angle (shown using three magnifications) of nanostructure on flat replica, microstructures, and hierarchical structure. Nano and hierarchical structures were fabricated with mass 0.8 μg mm^{-2} of lotus wax after storage for seven days at 50 °C with ethanol vapor.

into the replica material. A second and third replica of the same area was made to obtain negatives without contamination. For the positive replica, a liquid epoxy resin was used in the molding process.

To simulate a shark skin structure, a rib patterned surface was created using a FlashCut CNC milling machine(Dean 2009). Bechert *et al* (1997) have reported that for low drag the optimal groove depth for the rib surface should be about half of the lateral rib spacing. In the rib pattern design selected here, multiple stacks of ribs oriented along an axis were fabricated. For the fabrication, first a model of a rib patterned surface was designed in SolidWorks, and then the code for the rib's height, width, spacing and lengths, and channel dimensions was written using FeatureCAM in order to fabricate structures using the CNC milling machine. An acrylic resin was clamped onto the table of the CNC mill, and a fly cutter was used to make the top of the surface flat. The code was opened with FlashCut CNC and then the rib patterns were milled using an endmill with a 130 μm bit.

Figure 3(a) shows the SEM micrographs of the shark skin (*Squalus acanthias*) replica taken at a top view, a 45° tilt angle side view, and a 45° tilt angle top view. The shark skin replica shows that scales are lifted up at the end, and there are only three ribs on each scale. It is clearly visible that the V-shaped riblets' height varies between 200 and 500 μm, and their space varies between 100 and 300 μm. The ribs are oriented nearly parallel to the swimming direction of the sharks. Figure 3(b) shows the optical microscope images of the rib patterned surface fabricated as a model of artificial shark skin surface. The height, width, and length of the created ribs are 90, 38, and 850 μm, respectively. The spacing between the ribs is 180 μm.

2.2. Measurements of pressure drop

For the measurement of pressure drop using water and air flows, an experimental flow channel with a rectangular channel was designed and fabricated, as shown in figure 4. The fabricated surfaces were used for the upper and lower walls of the flow channel. Two pieces of plastic were glued between the upper and lower samples and at each end to prevent flow leak. For the measurement of pressure drop, the upper sample has two opening holes connected with a differential manometer (Model A 1000-13, Differential Pressure Plus Inc., USA). The thickness, width, and length of the resulting channel are designated as H, W, and L, respectively.

The inlet and outlet ports are machined and connected with plastic tubes. To introduce water into the channel in laminar flow, a syringe pump (Model NE-300, New Era Pump Systems Inc., USA) was used at a range of flow rates between 50 and 400 μl s^{-1} (a range of flow velocity between 0.03 and 0.23 m s^{-1}). The Reynolds number of the flow applied by the syringe pump is less than 300, which is laminar flow. To create a turbulent flow, a larger flow rate is needed than can be accomplished with the syringe pump. To accomplish high fluid flow, a separate plastic chamber filled with a measured amount of water was set to allow flow through the channel under the force of gravity. By measuring the amount of water and time to flow the water from a starting fluid level to an final fluid level, the Reynolds number was calculated as 4200 (flow velocity of 3.8 m s^{-1}), which indicates that the flow is turbulent using this

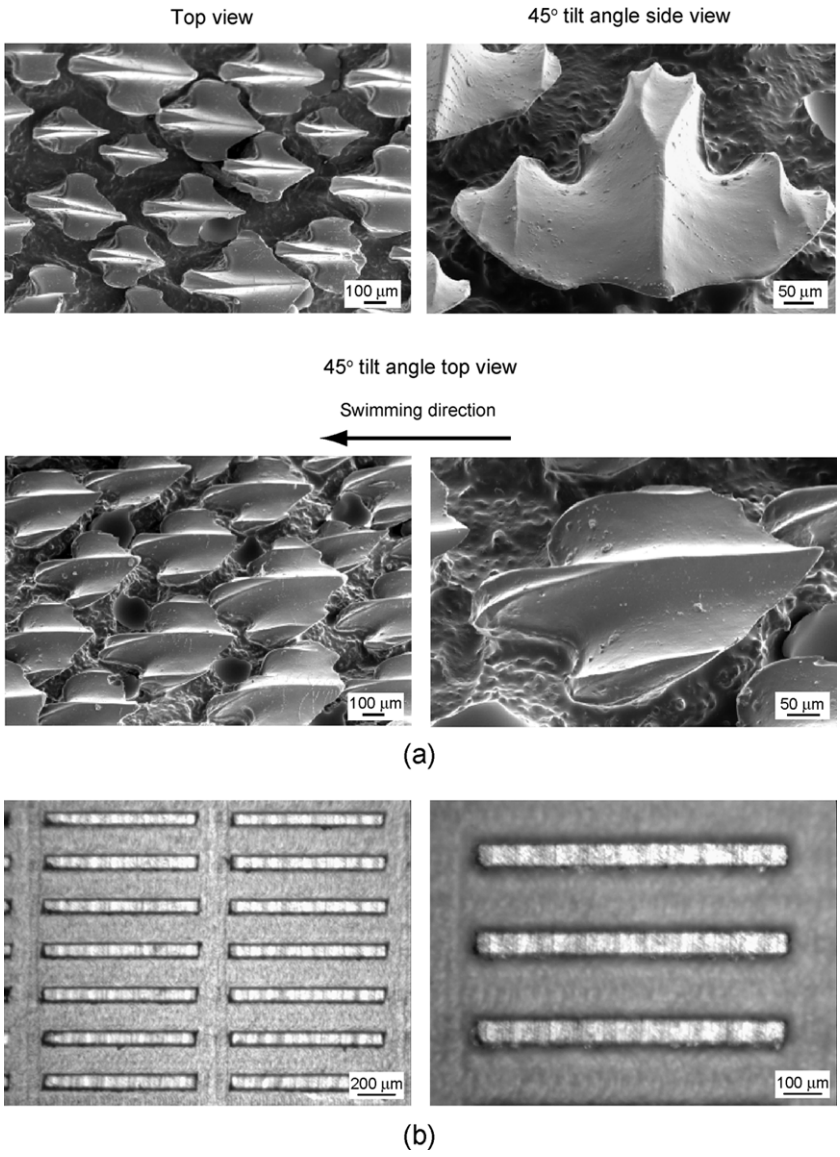

Figure 3. (a) SEM micrographs taken at top view, 45° tilt angle side view and 45° tilt angle top view, show the shark skin (*Squalus acanthias*) replica. The shark skin replica show only three ribs on each scale. It is clearly visible that the V-shaped riblets' height varies between 200–500 μm and their space varies between 100–300 μm, and (b) optical microscope images (shown using two magnifications) show the rib patterned surface fabricated as a model of artificial shark skin surfaces.

setup. In order to produce an air flow, laboratory air outlet was connected to the channel. A flowmeter (Model FL-1478-G, Omega Engineering, Inc., USA) was used to measure air flow rate between the laboratory air outlet and channel. For the experimental measurements of air flow, the calculated range of Reynolds number was between 200 and 4600, which indicates both laminar and turbulent flows.

2.3. Model for calculation of pressure drop and slip length

The pressure drop, Δp, of an incompressible fluid flow between two points along the channel of thickness, H, width, W, and length, L, for a hydrophilic flat surface can be calculated by (Blevins 1984)

$$\Delta p = \frac{\rho V^2 f L}{2D_{\mathrm{H}}}, \tag{1}$$

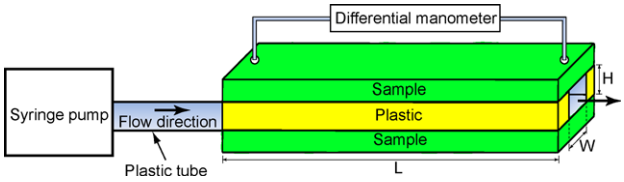

Figure 4. Schematic of the experimental flow channel connected with a differential manometer. The thickness, width, and length of the channel are H, W, and L, respectively.

(This figure is in colour only in the electronic version)

where ρ is the fluid density, V is the flow velocity obtained from flow rate (Q) divided by cross section area of the channel, and f is the friction factor which specifies the loss in pressure required to impel a flow over the surface or through the

channel. The friction factor is generally a function of Reynolds number, surface roughness, and the geometry of the surface. D_H is the hydraulic diameter which is proportional to four times the flow area divided by the perimeter of the surface containing the flow. For the rectangular channel, the hydraulic diameter is

$$D_H = \frac{2WH}{W+H}. \quad (2)$$

The friction factor for laminar flow is inversely proportional to the Reynolds number as (Blevins 1984)

$$f = \frac{k}{Re} \qquad \text{for laminar flow} \quad (3)$$

$$Re = \frac{\rho V D_H}{\eta}, \quad (4)$$

where η is the dynamic fluid viscosity. The Reynolds number can be used to determine whether the fluid flow will be within the laminar, turbulent, or transitional flow regimes. Since the Reynolds number is proportional to flow velocity, the pressure drop in laminar flow increases with flow velocity. k is the friction coefficient which can be found by the solution of Poisson's equation over the cross section as (Blevins 1984)

$$k = \frac{64}{\frac{2}{3} + \frac{11}{23}\frac{H}{W}(2 - \frac{H}{W})}. \quad (5)$$

From equation (5), the friction coefficient is dependent only on the shapes of the cross section but it is independent of surface roughness.

To improve the calculation of the friction factor for turbulent flow in a rectangular channel, Jones (1976) developed an improved equivalent diameter, $D_e = 64D_H/k$, and the friction factor for turbulent flow can be modified as

$$f = \frac{64}{Re} \qquad \text{for turbulent flow.} \quad (6)$$

Next, we present an analysis to calculate slip length in the laminar flow. Using the Navier slip boundary condition, the slip length b of the two infinite parallel and smooth plates can be obtained as (Blevins 1984, Ou *et al* 2004)

$$b = \frac{4\eta QL}{\Delta p W H^2} - \frac{H}{3}. \quad (7)$$

For a rectangular channel, the slip length would have the following general form (Ou *et al* 2004)

$$b = \frac{c\eta QL}{\Delta p W H^2} - \frac{H}{3}, \quad (8)$$

where c is a constant which needs to be obtained empirically. In order to obtain it, a pressure drop measurement on a hydrophilic channel needs to be made. Equation (8) is then fitted under the assumption of zero slip length with the measured pressure drop data to obtain c. It was found to be equal to 5 for the channel ($H = 0.7$ mm, $W = 2.5$ mm, $L = 60$ mm) used in this study. Now this equation is used to calculate the slip length for hydrophobic surfaces.

Table 1. Summary of the static contact angles and contact angle hysteresis measured on the various surfaces. Nanostructures and hierarchical structures were fabricated with 0.8 μg mm^{-2} of lotus wax after storage at 50 °C with ethanol vapor. The variation represents ±1 standard deviation.

	Static contact angle (deg)	Contact angle hysteresis (deg)
(a) Epoxy resin		
Flat epoxy resin	76 ± 0.9	67 ± 2.9 (151[a], 84[b])
Flat with thin wax layer	119 ± 2.4	56 ± 3.2 (148[a], 92[b])
Nanostructure	167 ± 0.7	6 ± 1.1 (170[a], 164[b])
Microstructure	160 ± 1.8	27 ± 2.1 (169[a], 142[b])
Hierarchical structure	173 ± 0.8	1 ± 0.6 (174[a], 173[b])
Shark skin replica	89 ± 1.7	66 ± 3.4 (155[a], 89[b])
(b) Acrylic resin		
Flat acrylic resin	82 ± 1.8	71 ± 2.6 (122[a], 51[b])
Rib patterned surface	146 ± 1.2	43 ± 1.2 (158[a], 115[b])

[a] Advancing contact angle.
[b] Receding contact angle.

3. Results and discussion

3.1. Wettability of various surfaces

To study the effect of lotus wax tubules on various surfaces for superhydrophobicity, the static contact angle and contact angle hysteresis were measured on flat, flat with thin wax layer, nanostructure, microstructure, and hierarchical surfaces (Bhushan *et al* 2009, Koch *et al* 2009b). The values measured for various surfaces are summarized in table 1. For static contact angle and contact angle hysteresis, droplets of about 5 μl in volume (with the diameter of a spherical droplet about 2.1 mm) were gently deposited on the surface using a microsyringe. For contact angle hysteresis, the advancing and receding contact angles were measured at the front and back of the droplet moving along the tilted surface, respectively. A static contact angle of 76° was found for flat epoxy resin. The microstructure (covered with a lotus wax film) has a static contact angle of 160°, but shows a much higher contact angle hysteresis of 27° than found in the hierarchical structure. Superhydrophobicity with a static contact angle of 167° and a contact angle hysteresis of 6° was also found in the nanostructured surface. Melting of the wax led to a flat surface with a flat wax film and a much lower static contact angle of 119° and higher contact angle hysteresis of 56°. The data of a flat lotus wax film on a flat replica show that the lotus wax by itself is hydrophobic. For the hierarchical structure, the highest static contact angles of 173° and lowest contact angle hysteresis of 1° were found. The recrystallized wax tubules are very similar to those of the original lotus leaf, but are 0.5–1 μm longer, the static contact angle is higher, and the contact angle hysteresis is lower than reported for the original lotus leaf (static contact angle of 164° and contact angle hysteresis of 3°).

To study the effect of the shark skin replica and rib patterned surface for superhydrophobicity, the static contact

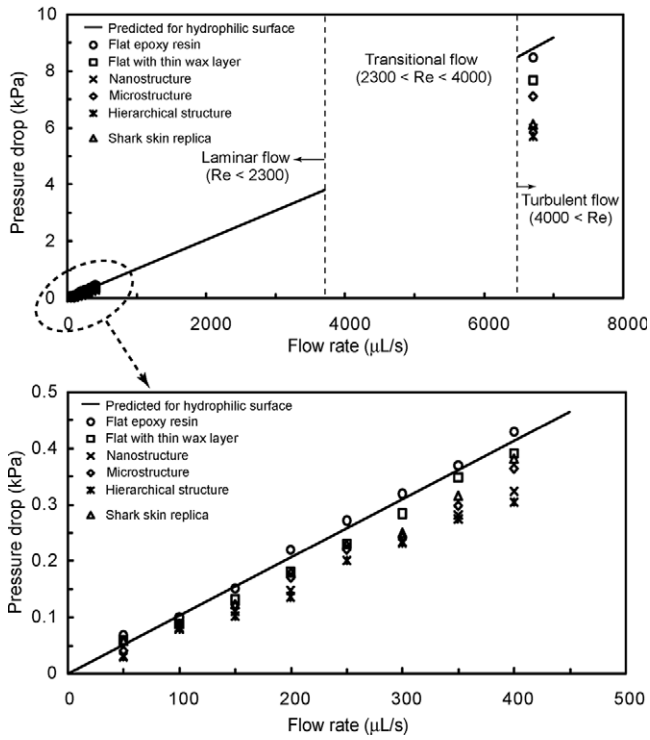

Figure 5. Pressure drop as a function of flow rate in the channel with various surfaces using water flow. The figure in the bottom is magnified for flow rates between 0 and 500 μl s^{-1}. Data are compared with predicted pressure drop values for a hydrophilic surface obtained using equation (1) for laminar and turbulent flows (solid lines).

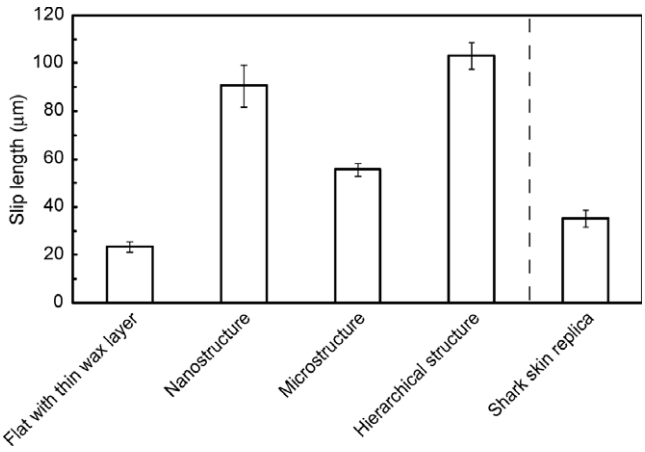

Figure 6. Bar chart showing the slip length in the channel with various surfaces using water flow in laminar flow ($0 < Re < 300$). The slip length was calculated using equation (8) and the pressure drop measured on various surfaces. The error bar represents ± 1 standard deviation.

angle and contact angle hysteresis were measured and are summarized in table 1. The shark skin replica had a static contact angle of 89° and a contact angle hysteresis of 66° for a water droplet. For acrylic resin material, a static contact angle of 82° was found for flat acrylic resin. Introduction of the rib patterns on the flat surface led to a much higher static contact angle of 146° and lower contact angle hysteresis of 43°.

3.2. Pressure drop in the channel using water flow and calculated slip length

To observe the fluid drag reduction in the channel using water flow, experiments on flat epoxy resin, flat with thin wax layer, nanostructure, microstructure, hierarchical structure, and shark skin replica were performed. In figure 4, the rectangular channels with these surfaces have dimensions of thickness $H = 0.7$ mm, width $W = 2.5$ mm, and length $L = 60$ mm. For calculation of the pressure drop using equation (1), the mass density (ρ) and viscosity (η) for water are taken to be 1000 kg m^{-3} and 0.001 Pa s, respectively (Lide 2009). Figure 5 shows the pressure drop as a function of flow rate in the channel with various surfaces using water flow. The measured data are compared with the predicted pressure drop values for a hydrophilic surface obtained using equation (1) for laminar and turbulent flows (solid lines). The figure in the bottom is magnified for flow rates between 0 and 500 μl s^{-1}. In both laminar and turbulent flows, the pressure drop increased linearly with flow rate for all samples. It was found that the pressure drop for the flat epoxy resin was similar to the value predicted by equation (1), while structured surfaces had values lower than the predicted. As mentioned earlier and shown in table 1, the introduction of roughness increases the hydrophobicity of the surfaces responsible for reduction in drag or pressure drop. The hierarchical structure with the highest contact angle and lowest static contact angle hysteresis provided the highest reduction of pressure drop. It is believed that air pockets inside the grooves underneath the fluid reduce the contact area between the fluid and the surface, resulting in a reduction of pressure drop. These results indicate that superhydrophobicity can lead to drag reduction in fluid flow.

As shown in figure 5, for shark skin replica, it was found that the pressure drop in laminar flow was higher than those of the nanostructure and hierarchical structures, and the reduction of pressure drop was about 12% as compared to the theoretical pressure drop. However, in turbulent flow, the reduction of pressure drop was similar to those of the nanostructure and hierarchical structures. Bechert *et al* (2000) showed that a turbulent boundary layer on the shark skin surface with ribs can help to reduce turbulent shear stress. The results of experimental measurements on shark skin replica showed that a reduction of pressure drop up to 30% was obtained in turbulent flow. It can be concluded that the surfaces with ribs are more beneficial in producing a drag reduction in turbulent flow than in laminar flow.

Based on a preliminary inspection of the pressure drop data, the slip length on the surfaces with different wettabilities was calculated using equation (8). For calculations, we assume that there is a no-slip boundary condition on flat epoxy resin, as verified from the experiments (Maali *et al* 2009). Figure 6 shows the bar chart showing the slip length in the channel with various surfaces using water flow in laminar flow ($0 < Re < 300$). The average values of slip length on the surfaces were calculated over all the experimental flow rates. A slip length of

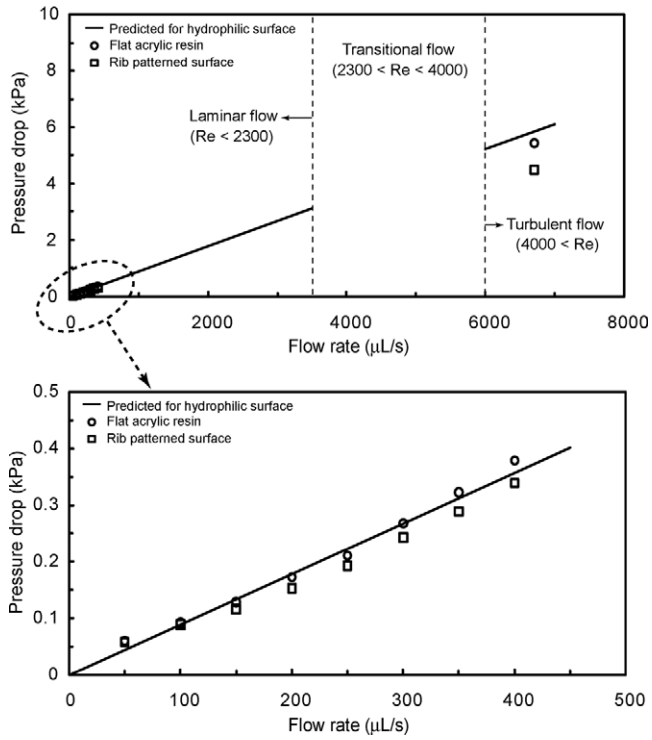

Figure 7. Pressure drop as a function of flow rate in the channel with flat acrylic resin and rib patterned surface using water flow. The figure in the bottom is magnified for flow rates between 0 and 500 μl s^{-1}. Data are compared with the predicted pressure drop values for a hydrophilic surface obtained using equation (1) for laminar and turbulent flows (solid lines).

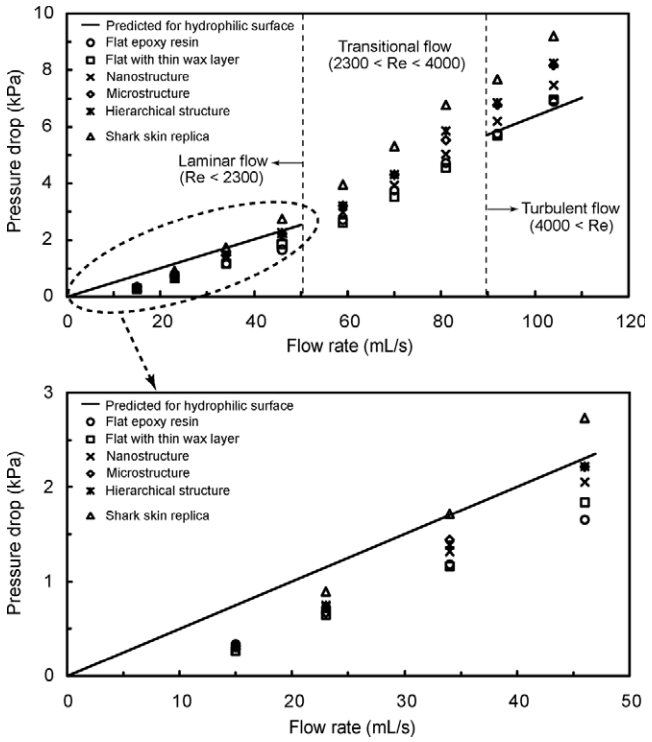

Figure 8. Pressure drop as a function of flow rate in the channel with various surfaces using air flow. The figure in the bottom is magnified for flow rates between 0 and 50 ml s^{-1}. Data are compared with predicted pressure drop values for a hydrophilic surface obtained using equation (1) for laminar and turbulent flows (solid lines).

24 μm was found for the flat surface with a thin wax layer. The microstructure (covered with a lotus wax film) and shark skin replica had slip lengths of 56 and 35 μm, but the nanostructure and hierarchical structures show much higher slip lengths of 91 and 103 μm, respectively, which implies the boundary slip increases with increasing hydrophobicity of solid surfaces. Zhu and Granick (2001) have reported that the slip length increases from the nanometer range to the micrometer range as the flow rate increases.

To observe the fluid drag reduction in the channel using water flow, experiments on flat acrylic resin and rib patterned surfaces fabricated as a model of artificial shark skin were also performed. In figure 4, the rectangular channels with these surfaces have dimensions of thickness $H = 1$ mm, width $W = 2$ mm, and length $L = 100$ mm. Figure 7 shows the pressure drop as a function of flow rate in the channel using water flow. The measured data are compared with predicted pressure drop values for a hydrophilic surface obtained using equation (1) for laminar and turbulent flows (solid lines). The figure in the bottom is magnified for flow rates between 0 and 500 μl s^{-1}. In laminar flow, it was found that the pressure drop increased linearly with flow rate and was similar to the value predicted by equation (1). However, in turbulent flow, a reduction of pressure drop was obtained up to 23% as compared to the theoretical pressure drop. This result shows a similar trend to that of the shark skin replica.

3.3. Pressure drop in the channel using air flow

To investigate the effects of air flow in the channel and compare them to water drag reduction, experiments with air flow on various surfaces were performed. In figure 4, the rectangular channels have dimensions of thickness $H = 0.7$ mm, width $W = 2.5$ mm, and length $L = 60$ mm. For the calculation of pressure drop using equation (1), the mass density (ρ) and viscosity (η) for air are taken to be 1.204 kg m^{-3} and 1.837×10^{-5} Pa s, respectively (Lide 2009). Figure 8 shows the pressure drop as a function of flow rate in the channel with various surfaces using air flow. The measured data are compared with predicted pressure drop values for a hydrophilic surface obtained using equation (1) for laminar and turbulent flows (solid lines). The figure in the bottom is magnified for flow rates between 0 and 50 ml s^{-1}. The pressure drop of the structured surfaces is higher than that of the hydrophilic surface in the turbulent flow, which is opposite to that in liquid flow. In both laminar and turbulent flows, the pressure drop increased linearly with flow rate for all samples. As mentioned earlier, in the case of water flow, air pockets between the structures reduce the contact area between the liquid and the surface, resulting in a reduction of the flow drag. The data shows that the structures are not beneficial for drag reduction in air flow. The introduction of roughness on the surfaces increases the pressure drop in the channel in the turbulent flow. It is generally known that surfaces with a streamlined body can produce dramatic reductions of the fluid pressure drag with

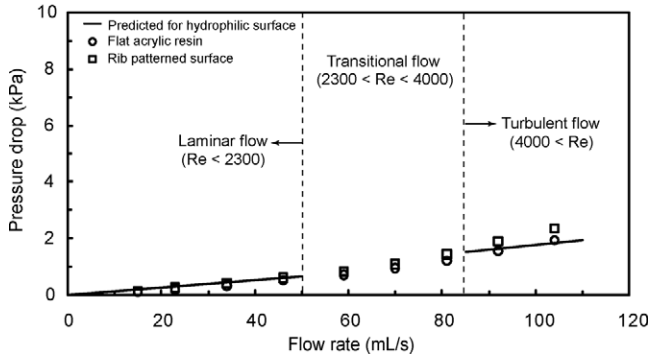

Figure 9. Pressure drop as a function of flow rate in the channel with flat acrylic resin and rib patterned surface using air flow. Data are compared with predicted pressure drop values for a hydrophilic surface obtained using equation (1) for laminar and turbulent flows (solid lines).

only a slight increase in shear stress in air flow (Bertin 1979). It is also known that as the Reynolds number increases, the pressure drop becomes very large, resulting in a larger pressure drag. The roughness structures on the surfaces may cause air to move around them, resulting in the formation of vortices and large fluid drag.

To observe the fluid drag reduction in the channel using air flow, experiments on flat acrylic resin and fabricated rib patterned surface were also performed. The rectangular channels with these surfaces have dimensions of thickness $H = 1$ mm, width $W = 2$ mm, and length $L = 100$ mm. Figure 9 shows the pressure drop as a function of flow rate in the channel with flat acrylic resin and rib patterned surface using air flow. The measured data are compared with predicted pressure drop values for a hydrophilic surface obtained using equation (1) for laminar and turbulent flows (solid lines). The experimental results show a similar trend to the data as shown in figure 8. It was found that the pressure drop of the rib patterned surface slightly increased due to the vortices formed at the end of the ribs in turbulent flow as compared to the theoretical pressure drop.

4. Conclusions

Drag reduction efficiency on biomimetic structured surfaces was investigated through pressure drop measurement in the channels using laminar and turbulent flows. The slip length for various surfaces in laminar flow was also investigated based on the measured pressure drop. It was found that the hierarchical structure with highest static contact angle and lowest contact angle hysteresis provided the highest reduction of pressure drop in both laminar and turbulent water flows, resulting in the highest slip length, followed by nanostructure and shark skin replica. These results indicate that superhydrophobicity can lead to drag reduction in water flow. It is also observed that drag reduction in turbulent flow with various structures is higher than that in laminar flow, with the largest drop in the case of shark skin replica. In the latter case, the reduction of pressure drop in turbulent flow was 30% and in laminar flow was 12%.

To investigate the effect of air flow in the channel and compare them to the water drag reduction, experiments with air flow on various surfaces were also performed. Unlike the result of water flow in the channel, the pressure drop of microstructure, hierarchical structure, and shark skin replica became higher than that of hydrophilic flat surfaces and nanostructure with increasing Reynolds number. The results indicate that these structures on the surfaces may cause air to move around them, resulting in the formation of vortices and large fluid drag in air flow.

Acknowledgments

The authors thank Professor Helmut Schmitz (Department of Zoology, University of Bonn) for providing the shark material, Anna Julia Schulte (Nees Institute for Biodiversity of Plants, University of Bonn) for the preparation of the negative replica, and Brian Dean and his group members (Ryan Allsop, Phillip Aquino, and Jonathan Lutz) as part of a course project at The Ohio State University for the preparation of the rib patterned surface.

References

Barthlott W and Neinhuis C 1997 Purity of the sacred lotus, or escape from contamination in biological surfaces *Planta* **202** 1–8

Batchelor G K 1970 *An Introduction to Fluid Dynamics* (Cambridge: Cambridge University Press)

Baudry J, Charlaix E, Tonck A and Mazuyer D 2001 Experimental evidence for a large slip effect at a nonwetting fluid–solid interface *Langmuir* **17** 5232–6

Bechert D W, Bruse M and Hage W 2000 Experiments with three-dimensional riblets as an idealized model of shark skin *Exp. Fluids* **28** 403–12

Bechert D W, Bruse M, Hage W, Van Der Hoeven J G T and Hoppe G 1997 Experiments on drag-reducing surfaces and their optimization with an adjustable geometry *J. Fluid Mech.* **338** 59–87

Bertin J J 1979 *Aerodynamics for Engineers* (Englewood Cliffs, NJ: Prentice-Hall)

Bhushan B 2007 *Springer Handbook of Nanotechnology* 2nd edn (Heidelberg: Springer)

Bhushan B 2009 Biomimetics: lessons from nature—an overview *Phil. Trans. R. Soc.* A **367** 1445–86

Bhushan B, Jung Y C and Koch K 2009 Micro-, nano- and hierarchical structures for superhydrophobicity, self-cleaning and low adhesion *Phil. Trans. R. Soc.* A **367** 1631–72

Blevins R D 1984 *Applied Fluid Dynamics Handbook* (New York: Van Nostrand-Reinhold)

Choi C-H and Kim C-J 2006 Large slip of aqueous liquid flow over a nanoengineered superhydrophobic surface *Phys. Rev. Lett.* **96** 066001

Chong M A S, Zheng Y B, Gao H and Tan L K 2006 Combinational template-assisted fabrication of hierarchically ordered nanowire arrays on substrates for device applications *Appl. Phys. Lett.* **89** 233104

Cortese B, Amone S D, Manca M, Viola I, Cingolani R and Gigli G 2008 Superhydrophobicity due to the hierarchical scale roughness of PDMS surfaces *Langmuir* **24** 2712–8

Cottin-Bizonne C, Barentin C, Charlaix E, Bocquet L and Barrat J L 2004 Dynamics of simple liquids at heterogeneous surfaces: molecular-dynamics simulations and hydrodynamic description *Eur. Phys. J.* E **15** 427–38

Cottin-Bizonne C, Cross B, Steinberger A and Charlaix E 2005 Boundary slip on smooth hydrophobic surfaces: intrinsic effects and possible artifacts *Phys. Rev. Lett.* **94** 056102
Dean B 2009 personal communications, The Ohio State University
del Campo A and Greiner C 2007 SU-8: a photoresist for high-aspect-ratio and 3D submicron lithography *J. Micromech. Microeng.* **17** R81–95
Genzer J and Efimenko K 2006 Recent developments in superhydrophobic surfaces and their relevance to marine fouling: a review *Biofouling* **22** 339–60
Goldstein S 1938 *Modern Development in Fluid Dynamics* (Oxford: Clarendon)
Goldstein S 1969 Fluid mechanics in first half of this century *Annu. Rev. Fluid Mech.* **1** 1–28
Honig C D F and Ducker W A 2007 No-slip hydrodynamic boundary condition for hydrophilic particles *Phys. Rev. Lett.* **98** 028305
Jones O C 1976 An improvement in the calculation of turbulent friction in rectangular ducts *J. Fluids Eng.* **98** 173–80
Joseph P, Cottin-Bizonne C, Benoit J M, Ybert C, Journet C, Tabeling P and Bocquet L 2006 Slippage of water past superhydrophobic carbon nanotube forests in microchannels *Phys. Rev. Lett.* **97** 156104
Koch K, Bhushan B and Barthlott W 2008 Diversity of structure, morphology, and wetting of plant surfaces (invited) *Soft Matter* **4** 1943–63
Koch K, Bhushan B and Barthlott W 2009a Multifunctional surface structures of plants: an inspiration for biomimetics (invited) *Prog. Mater. Sci.* **54** 137–78
Koch K, Bhushan B, Jung Y C and Barthlott W 2009b Fabrication of artificial lotus leaves and significance of hierarchical structure for superhydrophobicity and low adhesion *Soft Matter* **5** 1386–93
Kuan C Y, Hon M H, Chou J M and Leu I C 2009 Wetting characteristics on micro/nanostructured zinc oxide coatings *J. Electrochem. Soc.* **156** J32–6
Lauga E, Brenner M P and Stone H A 2005 *Handbook of Experimental Fluid Dynamics* (New York: Springer)
Lauga E and Stone H A 2003 Effective slip in pressure-driven Stokes flow *J. Fluid Mech.* **489** 55–77
Lide D R 2009 *CRC Handbook of Chemistry and Physics* 89th edn (Boca Raton, FL: CRC Press)
Maali A and Bhushan B 2008 Nanorheology and boundary slip in confined liquids using atomic force microscopy *J. Phys.: Condens. Matter* **20** 315201
Maali A, Wang Y and Bhushan B 2009 Evidence of the no-slip boundary condition of water flow between hydrophilic surfaces using atomic force microscopy *Langmuir* **25** 12002–5
Ming W, Wu D, van Benthem R and de With G 2005 Superhydrophobic films from raspberry-like particles *Nano Lett.* **5** 2298–301
Neto C, Evans D R, Bonaccurso E, Butt H-J and Carig V S J 2005 Boundary slip in Newtonian liquids: a review of experimental studies *Rep. Prog. Phys.* **68** 2859–97
Ou J, Perot B and Rothstein J P 2004 Laminar drag reduction in microchannels using ultrahydrophobic surfaces *Phys. Fluids* **16** 4635–43
Sbragaglia M and Prosperetti A 2007 Effective velocity boundary condition at a mixed slip surface *J. Fluid Mech.* **578** 435–51
Shirtcliffe N J, McHale G, Newton M I, Chabrol G and Perry C C 2004 Dual-scale roughness produces unusually water-repellent surfaces *Adv. Mater.* **16** 1929–32
Stokes S G G 1851 On the effect of the internal friction of fluids on the motion of pendulums *Trans. Camb. Phil. Soc.* **9** 8–106
Sun M, Luo C, Xu L, Ji H, Ouyang Q, Yu D and Chen Y 2005 Artificial lotus leaf by nanocasting *Langmuir* **21** 8978–81
Tretheway D C and Meinhart C D 2002 Apparent fluid slip at hydrophobic microchannel walls *Phys. Fluids* **14** L9–12
Vinogradova O I and Yakubov G E 2003 Dynamic effects on force measurements. 2. Lubrication and the atomic force microscope *Langmuir* **19** 1227–34
Wang Y, Bhushan B and Maali A 2009 Atomic force microscopy measurement of boundary slip on hydrophilic, hydrophobic, and superhydrophobic surfaces *J. Vac. Sci. Technol.* A **27** 754–60
Watts E T, Krim J and Widom A 1990 Experimental-observation of interfacial slippage at the boundary of molecularly thin-films with gold substrates *Phys. Rev.* B **41** 3466–72
Zhao Y, Li M, Lu Q and Shi Z 2008 Superhydrophobic polyimide films with a hierarchical topography: combined replica molding and layer-by-layer assembly *Langmuir* **24** 12651–7
Zhu X and Granick S 2001 Rate-dependent slip of Newtonian liquid at smooth surfaces *Phys. Rev. Lett.* **87** 096105
Zhu Y and Granick S 2002 Limits of the hydrodynamic no-slip boundary condition *Phys. Rev. Lett.* **88** 106102